Exploring Flux Representations of Complex Kinetics Networks

Kaiyuan He, Marianthi G. Ierapetritou, and Ioannis P. Androulakis
Dept. of Chemical and Biochemical Engineering, Rutgers, The State University of New Jersey, Piscataway, NJ 08854

DOI 10.1002/aic.12608
Published online May 17, 2011 in Wiley Online Library (wileyonlinelibrary.com).

To extract meaningful information from complex kinetic models involving a large number of species and reactions, advanced computational techniques are required. In this work, new approaches have been proposed based on element flux calculations for systematic kinetic analysis of complex reaction models. These approaches quantify element transformation flux between species to determine a metric that accurately captures the production and consumption of species. Furthermore, a graph searching procedure is employed to retrieve all possible reaction pathways from the highly complex reaction networks. Element fluxes involved in these pathways provide an indicator to quantitatively evaluate pathway activities. Based on pathway activities, a novel approach is proposed to project the totality of the information contained in pathway weights onto a single scalar, reactivity status indicator, which enables a compact representation of local chemistry. The proposed approaches are illustrated with highly complex kinetic mechanisms describing oxidation of n-*pentane,* n-*heptane, and a biodiesel surrogate methyl-butanoate*. © 2011 American Institute of Chemical Engineers *AIChE J,* 58: 553–567, 2012

Keywords: reaction kinetics, combustion (biofuels and fuel mixes)

Introduction

To make accurate predictions of processes involving complex reaction systems, numerous detailed chemical mechanisms consisting of thousands of species and tens of thousands of reactions have been developed for a wide range of applications.[1–8] As the kinetic models are developed to describe more complex systems for a wide range of applications, the reaction mechanisms will continue to increase in size. Both the development and the implementation of the detailed mechanisms require the understanding of species and reaction pathways through kinetic analysis. However, the large mechanism sizes make it difficult to perform a detailed kinetic analysis of the system. To identify and extract kinetically important species and reactions from detailed reaction mechanisms, a number of kinetic analysis approaches have been proposed. A commonly used kinetic analysis method is the sensitivity analysis approach.[9–11] Sensitivity analysis approaches investigate the effects of parameter or variable change on the solution of the mathematical model. One example is to calculate local sensitivity of species concentrations on individual reaction parameters.[11–13] However, the parameter perturbation considered in local sensitivity analysis is quite small, whereas time dependent sensitivity analysis was proposed in more recent study which enables the illustration of the sensitivity between species in a graphical representation.[14,15] Based on the sensitivity analysis results, a plot of reaction pathways can be constructed, representing the evolution of species from reactants to products. One of the program packages for semiautomatic generation of pathway plots is the XSENKPLOT program developed by NIST.[16] This program provides a graphical representation of reaction pathways given a user-specified important species set. The methodology, however, relies on the identification of important species which is not a simple task. To overcome the limitations of conventional sensitivity analysis, an automatic pathway plotting method was developed by Bendtsen et al.,[17] which identifies important species

Correspondence concerning this article should be addressed to I. P. Androulakis at yannis@rci.rutgers.edu.

based on their contribution to the conversion rates of given reactants or products.

In this article, new kinetic analysis approaches have been proposed based on element flux, including species analysis, pathway analysis, and compact representations of local chemistry. The program retrieves thermodynamic and kinetic variables from CHEMKIN[18] based simulation programs and calculates element transformation flux from reactants to intermediates and finally products over specific time intervals.[19,20] A detailed description of element flux calculation is available in Ref. [21]. Based on the element flux calculation, two types of kinetic analysis are performed, targeting species and pathways, respectively. The species analysis identifies important species over the entire process or within specific time interval. In addition, by tracing the influx and/or outflux of each species, the behavior of individual species can be correlated to the evolution of the entire system. This facilitates the investigation of species that are representative to specific system behaviors. For the pathway analysis, a graph searching technique is employed to retrieve pathways between given species and a weight propagation procedure is introduced to quantify the importance of each pathway on a normalized scale. This allows the quantification of contributions of different pathways as well as the comparison of pathways between different systems.

In the next section, we describe the algorithms of the program package and subsequently use *n*-pentane and methylbutanoate oxidation mechanisms as examples to illustrate the program. It should be noted that using these two mechanisms is not to validate or compare the mechanisms, but rather to use them as examples to demonstrate how element flux analysis can effectively capture the chemical characteristics of a kinetic mechanism. The examples cover a wide range of reacting conditions and represent both hydrocarbon and oxygenated fuel combustion.

Formulation of Element Flux Analysis

The element flux analysis provides a metric to quantify the activity of species in terms of element transformation between sources and sinks. The instantaneous element flux pointer of atom A (such as C, H, O, N, etc.) from species j to species k through reaction i, denoted as $\dot{A}_{ijk}$, is defined in Eq. 1.[19] $\dot{A}_{ijk}$ is positive when reaction i is proceeding from species j to k and negative if the reverse transformation takes place. The total instantaneous flux from species j to species k can be calculated by summing $\dot{A}_{ijk}$ over all the reactions in which species j and k are involved, as represented in Eq. 2.

$$\dot{A}_{ijk}(t) = q_i(t)\frac{n_{A,j}n_{A,k}}{N_{A,i}} \tag{1}$$

$$\overline{\dot{A}}_{jk}(t) = \sum_{i=1}^{N_R} \dot{A}_{ijk}(t) \tag{2}$$

where $q_i(t)$ is the instantaneous rate of reaction i (mol/s), $n_{A,j}$ is the number of atoms A in species j, $n_{A,k}$ is the number of atoms A in species k, $N_{A,i}$ is the total number of atoms A in reaction i, and N_R represents the number of reactions that these species participate as reactants or products. It is should be noted that the element flux between two species obtained from Eqs. 1 and 2 may involve more than one reaction. Thus the metric derived in the proposed element flux analysis approach represents the total element transformation between two species through all reactions that involve them.

In our previous study,[22] it was found that quantification of element flux based on net reaction rates $q_i(t)$ results in erroneous calculation of element transformation involving species in quasi-steady-state and partial-equilibrium reactions. This is due to the fact that for quasi-steady-state species, their influx and outflux are both large while the net flux is small. Small net flux also stems from partial-equilibrium reactions. Species involved in partial equilibrium reactions have fast element transformation through forward and reverse reactions. However, the net reaction rates are of much smaller magnitudes which results in small element fluxes according to Eq. 1. Since the element flux analysis is based on the assumption that large flux represents leading transitions while small flux indicates species of less importance, incorrect calculation of flux of quasi-steady-state species and partial-equilibrium reactions will underestimate the activity of the involved species. It should be emphasized that although quasi-steady-state species and partial-equilibrium reactions are often eliminated in mechanism reduction approaches, they are not redundant and their evolution are defined by the corresponding algebraic relations instead of kinetic differential equations.[23] To avoid underestimation of the importance of species involved in quasi-steady state and partial equilibrium reactions, absolute values of both forward and reverse reactions are taken into account in flux calculation as follows:

$$\dot{A}_{ijk}(t) = (|q_{i\text{fwd}}(t)| + |q_{i\text{rev}}(t)|)\frac{n_{A,j}n_{A,k}}{N_{A,i}} \tag{3}$$

where $q_{i\text{fwd}}$ and $q_{i\text{rev}}$ are the reactions rates of forward and reverse reaction, respectively.

The flux values defined in Eq. 3 are functions of time. By repeating the analysis at preselected time instances, one can capture instantaneous element transformations. This is equivalent to taking snapshots during the reaction process and identifying, on-the-fly, active sources and sinks. These connections can then be used to identify reaction pathways as well as their dynamic evolution over time. However, the instantaneous flux describes only the local reactive characteristics, which makes it difficult to derive global information. To address this limitation, a time-integrated flux indicator is proposed. The main idea is to derive over time an indicator for a source-sink combination based on integration of instantaneous flux defined in Eq. 3. Therefore, we define the time-integrated flux indicator as follows:

$$\hat{\dot{A}}_{jk} = \int_{t=0}^{\tau} \overline{\dot{A}}_{jk}(t)dt \tag{4}$$

The integral in Eq. 4 is estimated numerically by summing the instantaneous pointers at all the time instances as the integrator generates them. In this way, the entire reaction trajectory is considered. The indicator defined in Eq. 4 assigns a unique, overall number to each source-sink pair, which is representative for the entire reaction period.

The purpose of time-integrated element flux analysis is to establish "global" insight into the reaction pathways. It allows for a comprehensive and macroscopic view of the

Table 1. Time-Integrated Carbon (C) Flux of Characteristic Species in Methyl Butanoate and *n*-pentane Oxidation at Different Initial Temperatures

	Methyl Butanoate			*N*-pentane		
	From	To	Relative C Flux	From	To	Relative C Flux
$T_0 = 650$ K	CO	CO2	1.00E+00	CO	CO2	1.00E+00
	MP2D	C2H3CO	1.06E-02	CH3CO	CO	3.79E-02
	C2H2	HCCO	7.51E-03	NC5H12	C5H11–2	1.12E-02
	C2H3CO	C2H3	5.03E-03	C5H11–2	C5H11O2–2	4.88E-03
	MB2J	MP2D	1.97E-03	C5H11–2	C3H6	3.87E-03
	MB	MB2J	1.83E-03	C3H6	CH3CHCO	2.78E-03
	MB4OOH2J	MBCY4O2	1.79E-05	C5H11O2–2	C5H10OOH2–4	2.72E-03
	C3H6	C3H5-A	9.90E-06	C5H10OOH2–4O2	NC5KET24	1.93E-03
	MB2OOH4OO	MB4OOH2*O	6.88E-06	C5H10OOH2–4	C5H10OOH2–4O2	1.85E-03
	MB2OOH4J	MB2OOH4OO	5.83E-07	C5H10OOH2–4	C5H10O2–4	7.47E-04
$T_0 = 950$ K	CO	CO2	1.00E+00	CO	CO2	1.00E+00
	MP2D	C2H3CO	1.95E-02	C2H2	HCCO	2.72E-01
	C2H3CO	CO	1.71E-02	C2H4	CH3	5.61E-02
	C3H5-A	C3H4-A	3.63E-03	C3H6	C3H5-A	2.07E-02
	MB	MB2J	3.51E-03	NC3H7	C2H4	4.56E-03
	MB2J	MP2D	2.89E-03	NC5H12	C5H11–2	4.14E-03
	MB2OOH4J	MBCY4O2	3.10E-05	C4H6	C2H4	4.13E-03
	MB2OO	MB2OOH4J	1.68E-06	C5H11–2	C3H6	2.69E-03
	MB2OOH4J	MB2OOH4OO	1.06E-07	C5H11–2	C2H5	1.79E-03
	MB2OOH4OO	MB2OOH2*O	8.20E-08	C5H11–1	NC3H7	1.14E-03

Carbon flux pointers are normalized to the largest pointer in the scheme to enable comparison between different schemes.

reactant transformation to intermediates and finally to products. In the next section, the way the element flux analysis is implemented in computational simulations is introduced.

Computer Implementation of Element Flux Analysis

The proposed element flux analysis calculates element transformation between species based on reaction rates and stoichiometric coefficients of the system. In this work, the thermodynamic properties and reaction rates definitions are handled using CHEMKIN.[18] To illustrate the way element flux analysis is implemented, we have provided in Appendix A a FORTRAN pseudocode in which standard CHEMKIN nomenclature is used. The maximum number of source-sink pairs that have element transfer is $N_{\text{species}} \times N_{\text{species}}$. Thus the main computation task of the method is the calculation and storage of an $N_{\text{species}} \times N_{\text{species}}$ matrix where each entry represents the element flux between two species. However, this matrix is usually sparse due to the fact that each species is only connected to a small number of species through reactions. To avoid unnecessary CPU time looping over species pairs that are not connected, a loop over all reactions is employed instead of a two-level loop over all species. Since the number of species included in each reaction is limited, the flux analysis is scaled to the number of reactions in the mechanism while traditional sensitivity analysis is scaled as $N_{\text{species}} \times N_{\text{species}}$. Efficient flux calculation is especially beneficial when the analysis is performed on-the-fly in realistic flow calculations.[21,24]

The flux is calculated at every time step (IT) through a loop over all reactions (NII) and all species participating in each reaction (K and K1). If such a pair of species participate in the same reaction and contain the element of interest (denoted as NCF(NELE, K) .GT. 0), their stoichiometric coefficients are checked to determine if they have a reactant/product relationship (ISTOIC*ISTOIC1 .LT. 0). The forward and reverse reaction rates (Qfwd and Qrev) and the number of element atoms (NAJ, NAK, and NAI) are used to determine the temporal flux pointer AJK(IFROM, ITO, t). As the instantaneous flux pointers AJK(IFROM, ITO, t) are generated, they are numerically integrated to obtain the time-integrated flux pointer which indicates the total element transformation flux between species.

Once the flux pointers are obtained, the following kinetic analysis can be performed.

Species Analysis

The first level of kinetic analysis carried out illustrates the importance of species in terms of sources and sinks in element transformation. Simply by sorting the pairs in descending order, we can identify leading transitions represented by large flux. If time-integrated flux data are considered, leading transitions reveal globally crucial species that play vital roles in the overall reaction process. On the other hand, if instantaneous flux pointers are used, locally active species can be identified, representing local reaction characteristics. To better illustrate this idea, two mechanisms are analyzed in this section:

(1) Biodiesel surrogate methyl-butanoate mechanism (264 species and 1219 reactions).[3]

(2) *N*-pentane oxidation mechanism (385 species and 1895 reactions).[1]

These two mechanisms are selected because they describe oxygenated fuel and hydrocarbon fuel oxidation, respectively, and the mechanisms are fairly large to demonstrate the capability of the analysis approach in retrieving meaningful kinetic information from complex mechanisms. The flux analysis is carried out in an adiabatic plug flow reactor (PFR) simulation. The calculations are performed using stoichiometric conditions at 650 K and 950 K to represent oxidation at low and high temperature.[1,19,25] Table 1 summarizes the time-integrated carbon flux

Table 2. Instantaneous Carbon (C) Flux of Methyl Butanoate and *n*-pentane Oxidation at Different Stages with Initial Temperature 650 K

	Methyl Butanoate			*N*-pentane		
	From	To	C Flux	From	To	C Flux
Initial stage $T = 675$ K	MB2J	MB2OO	7.36E-01	C5H11–2	C5H11O2–2	8.34E+00
	MB	MB2J	7.06E-01	NC5H12	C5H11–2	8.30E+00
	MB3J	MB3OO	3.82E-01	C5H11O2–2	C5H10OOH2–4	4.19E+00
	MB	MB3J	3.74E-01	C5H10OOH2–4	C5H10OOH2–4O2	4.17E+00
	MB2O	C2H5CHO	2.76E-01	C5H11–3	C5H11O2–3	4.16E+00
	MB2OOH	MB2O	2.59E-01	NC5H12	C5H11–1	4.15E+00
	MB3OO	MB3OOH2J	2.48E-01	C5H11–1	C5H11O2–1	4.15E+00
	MB3OOH2J	MB2D	2.42E-01	NC5H12	C5H11–3	4.14E+00
	MB4J	MB4OO	2.27E-01	C5H10OOH2–4O2	NC5KET24	4.11E+00
	MB2OO	MB2OOH	2.05E-01	C5H10OOH2–4	C5H10O2–4	2.00E+00
Intermediate stage $T = 1550$ K	HCO	CO	1.12E+03	HCO	CO	9.75E+02
	CH2O	HCO	8.52E+02	CH2O	HCO	7.51E+02
	MB2D	C5H7O2	4.08E+02	C3H6	C3H5-A	4.32E+02
	CH3O	CH2O	4.00E+02	C3H5-A	C3H5O	3.32E+02
	C5H7O2	CH2CHCHCO	3.89E+02	CH3CO	CO	2.99E+02
	MP2D	C2H3CO	3.63E+02	CH3CHO	CH3CO	2.89E+02
	C2H3O1,2	CH3CO	3.02E+02	CH3CO	CH3	2.84E+02
	CH2CHO	C2H3O1,2	2.97E+02	C2H5	C2H5O	2.70E+02
	C2H3CO	C2H3	2.88E+02	C2H3O1,2	CH3CO	2.65E+02
	CH3CO	CO	2.25E+02	CH2CHO	C2H3O1,2	2.60E+02
Final stage $T = 2550$ K	CO	CO2	3.50E+04	CO	CO2	5.05E+04
	SC3H5OCH2	C3H5-S	2.51E+03	HCO	CO	2.46E+04
	C3H5-S	C3H4-P	2.05E+03	CH2O	HCO	2.08E+04
	HCO	CO	1.63E+03	CH3	CH2O	1.35E+04
	CH2O	HCO	1.50E+03	C2H2	HCCO	1.20E+04
	C3H4-P	C3H3	1.38E+03	CH4	CH3	8.91E+03
	C3H3	C3H2	1.14E+03	HCCO	CO	8.54E+03
	HCCO	CO	9.61E+02	C2H3	C2H2	6.68E+03
	C2H2	HCCO	9.23E+02	C2H4	C2H3	5.31E+03
	SC3H5OCH2	CH2O	8.37E+02	HCCO	CH2(S)	4.38E+03

between species of methyl-butanoate and *n*-pentane oxidation. The first two columns represent the FROM and TO species of element transformation. To be consistent, the species naming conventions are the same as in the original mechanisms (see Appendix B). The third column is the time-integrated flux data. Nearly 2000 source-sink connections have been identified for the entire mechanism. However, due to the space limitations, only species with large element flux are listed. Characteristic species of methyl-butanoate oxidation includes hydroperoxy alkylperoxy radical (MB2OOH4OO), cyclic ether (MBCY4O2), and methyl propenoate (MP2D). Hydroperoxy alkylperoxy radical (MB2OOH4OO) is formed by addition of a second oxygen molecule to the hydroperoxyalkyl radical (MB2OOH4J), which stems from initial radical (MB2J). The second oxygen addition to initial radicals is a typical low temperature oxidation procedure.[3] Cyclic ether MBCY4O2 is the product of decomposition of MB2OOH4J, which competes with second oxygen addition. Methyl propenoate MP2D is the product of beta scission of the carbon chain of methyl butanoate and has the largest contribution to the original reactant oxidation. The identification of these source-sink connections in flux analysis reveals that there is competition between unimolecular decomposition and second oxygen addition in methyl butanoate oxidation. Another observation is that low temperature and high temperature oxidations of methyl butanoate have qualitatively very similar active species. However, the relative magnitude of element flux between sources and sinks establishes the fundamental difference between the two cases.

The flux analysis of *n*-pentane oxidation indicates that the shift between unimolecular decomposition and second oxygen addition as temperature increases is higher compared to methyl butanoate. At 650 K, active species of *n*-pentane oxidation include hydroperoxy alkylperoxy radical $C_5H_{10}OOH2\text{-}4O2$, which is formed from second oxygen addition to hydroperoxyalkyl radical $C_5H_{10}OOH2\text{-}4$, cyclic ether $C_5H_{10}O2\text{-}4$, the product of $C_5H_{10}OOH2\text{-}4$ decomposition, and C_3H_6, from beta scission. However, as temperature increases to 950 K, only species on beta scission pathways, e.g., C_3H_6, C_2H_5, etc., are identified. This shift from oxygen addition pathways to beta scission pathways as temperature increases indicates that the *n*-pentane oxidation pathways are more sensitive to temperature changes than methyl butanoate oxidation.

Time-integrated flux identifies globally important species for the entire reaction process, compared with the instantaneous flux calculation that provides information about the specific stage of the oxidation process. Table 2 summarizes the instantaneous flux of methyl butanoate and *n*-pentane oxidations. As shown in Table 2, sources and sinks vary significantly at different stages of the oxidation process. For example, at the initial stage, fuel decomposition and oxidation are the main component of the combustion process. As the system proceeds, generation and oxidation of small species dominate the reaction process. When the system evolves to the final stage, the oxidation of very small species such as HCCO and CO becomes the dominant reactions.

Species analysis based on element flux in terms of sources and sinks provides a useful tool to measure species activity, which can be further implemented in redundant species identification. Therefore, the species analysis method also

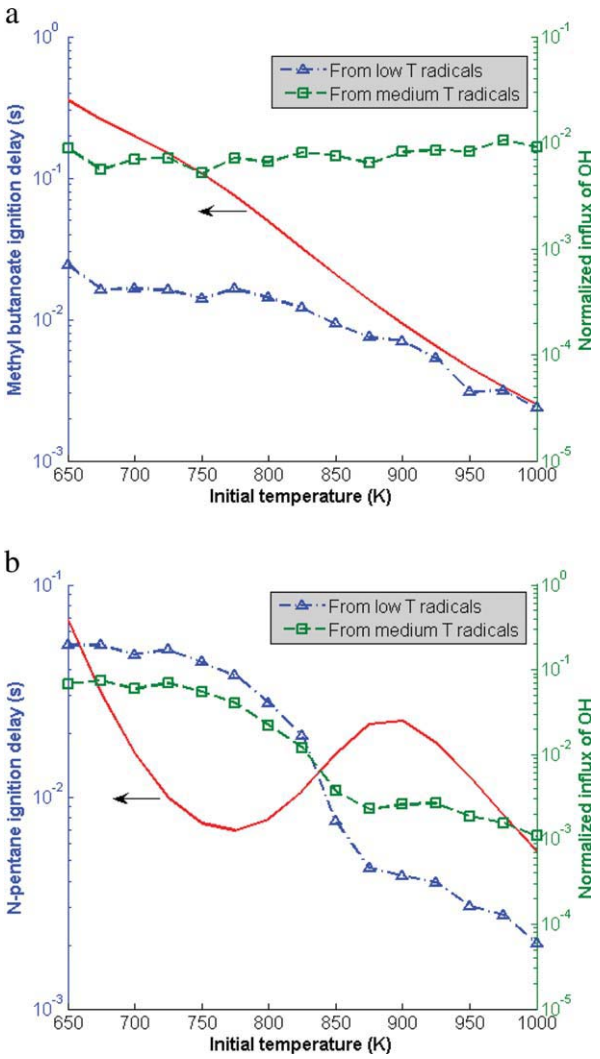

Figure 1. OH influx from second oxygen addition (low T) and hydroperoxyalkyl radicals decomposition (medium T).

(a) methyl butanoate oxidation, (b) *n*-pentane oxidation. $P0 = 9.6$ atm, $\phi = 1.0$. [Color figure can be viewed in the online issue, which is available at wileyonlinelibrary.com.]

provides a foundation for mechanism reduction procedures. Both skeletal reduction and dynamical reduction techniques have been proposed based on species flux analysis, which are recently discussed in Refs. [19] and [21].

Given the element flux between sources and sinks, the total influx and outflux of each species can be obtained to represent its production and consumption rates. This enables further options of the program: tracing the dynamic accumulation and consumption of species during the system evolution. This analysis can be performed on key radicals or species of specific interest to investigate their correlation with system behaviors. Taking the OH radical for example, in both methyl butanoate and *n*-pentane oxidation systems, OH plays an important role in the chain branching and chain propagation pathways.[1,3,25] Thus analyzing the influx and outflux of OH captures the oxidation rates of the system. In *n*-pentane oxidation systems, chain branching pathways induced by second oxygen addition to hydroperoxyalkyl radicals increase the concentration of OH, thus having a particular important effect on the low temperature oxidation rates. However, as the temperature increases, unimolecular decomposition of hydroperoxyalkyl radicals and hydrocarbons become favored, which lead almost exclusively to chain propagation reactions. The shift between second oxygen addition and unimolecular decomposition as the temperature increases is the cause of the negative temperature coefficient (NTC) behavior.[1] Since the OH production rate is much lower in unimolecular decomposition compare with second oxygen addition, analyzing the influx of OH provides an insight of the NTC behavior. Figure 1 shows the contribution of second oxygen addition radicals and hydroperoxyalkyl radicals, which represent low T oxidation and medium T oxidation respectively, to OH production in the system from 650 K to 1000 K. The influx of OH from low T and medium T radicals are normalized to the total influx of OH to reveal their respective contributions. Ignition delay at each temperature is compared with OH influx to illustrate the correlation between them. As shown in Figure 1, OH production from second oxygen addition radicals and hydroperoxyalkyl radicals only have small contribution to OH production and changes modestly with temperature. This is due to the fact that the oxidation of oxygenated contents (e.g., ester group in methyl butanoate) dominates the OH production, which does not have NTC behavior. On the other hand, OH production in *n*-pentane oxidation shows strong temperature dependence, resulting in a distinct NTC behavior of ignition delay time. At low temperature, approximately one-third of OH is generated from second oxygen oxidation radicals and hydroperoxyalkyl radicals. As the temperature increases above 775 K, second oxygen addition and hydroperoxyalkyl radical decomposition become less favorable, which reduces the radical pool and subsequently lowers the overall oxidation rate. At high temperature, beta scission becomes dominant and defines the overall oxidation rate, which reduces the NTC effects. It can be observed in Figure 1 that the OH influx change accurately captures the temperature range of ignition delay NTC behavior. The flux analysis on OH reveals the underlying chemical phenomena of NTC behavior, that is, the competition between chain-branching second oxygen oxidation pathways, chain propagation hydroperoxyalkyl radical decomposition pathways, and chain propagation beta scission pathways.[1,3,19,25]

Although we selected to study the OH radical activity and the pathways of fuel oxidation in the analysis, the proposed method can be extended to any species and pathways of interest. While species analysis provides an indicator to identify active species and measure their contribution to system's transitions, they do not describe the overall pathways that the reaction system evolves through. Therefore, in the kinetic analysis program package, a pathway analysis procedure is introduced to retrieve pathway information from a complex reaction network and quantify pathway activities based on element flux analysis.

Pathway analysis

Another valuable output of the program is the identification of individual pathways and the quantification of their activities. The element flux indicators provided by flux

	FROM	TO	Flux
1	A	B	150
2	A	C	200
3	A	F	50
4	B	D	5
5	B	E	8
6	C	D	1
7	D	E	3
8	D	F	2
9	E	F	10

	Pathways
1	ABDF
2	ACDF
3	ABDEF
4	ACDEF
5	ABEF
6	AF

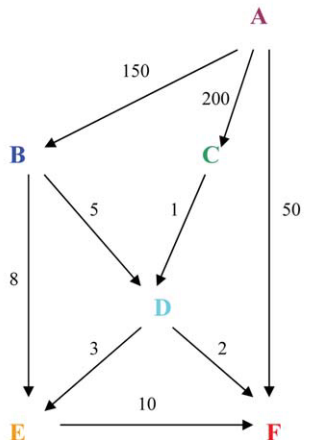

Figure 2. Pathway identification and visualization based on element flux indicators.

[Color figure can be viewed in the online issue, which is available at wileyonlinelibrary.com.]

analysis describe the transition between two species and illustrate important connections between fuels and final products. Given this information between sources and sinks, a Breadth First Search (BFS) algorithm[26] can be employed to identify the reaction pathways. The BFS algorithm initiates from initial species (e.g., fuels) and find all species that are connected to the initial species. These newly found species are stored in the algorithm as second level species, which serves as initial species in the next searching step. The search algorithm repeats the breadth first searching until no further species can be identified. An illustrative example of pathway identification is given in Figure 2, where all possible pathways are identified based on the connection information between species and visualized in a flux graph. Note that since this example is shown for illustration purposes only, material balances are not enforced in this system.

The pathways identified from flux analysis provide qualitative connections between reactants and products. However, to analyze pathway activities, a quantitative procedure needs to be developed. Based on the flux analysis, we propose to use the normalized flux values to quantify the weight of each pathway. In the proposed method, the influx/outflux of each species from/to different species are normalized to the total influx/outflux of this species to evaluate the contribution of each connection. Taking the system in Figure 2 for example, when the consumption pathways of A is examined, the calculation initiates from A and all its outflux connections, AB, AC, and AF, are normalized to the total out flux of species A (400), which gives the weight of each connection as shown in Figure 3a. Then the calculation proceeds to species B, C, and F. The two outflux connections of species B (BE and BD) are normalized to the total out flux of B (13), while the only outflux from C (CD) is given the weight of 1. Since F does not have outflux connection, no outflux normalization is needed. The normalization procedure then proceeds until no further outflux connection is found. On the other hand, if the production pathways of F are to be analyzed, the calculation initiates from F and all its influx connects are normalized. Three influxes of F can be identified in the system, and they are normalized to the total influx of F (62), giving normalized weight as shown in Figure 3b. The normalization procedure proceeds until no further influx can be identified.

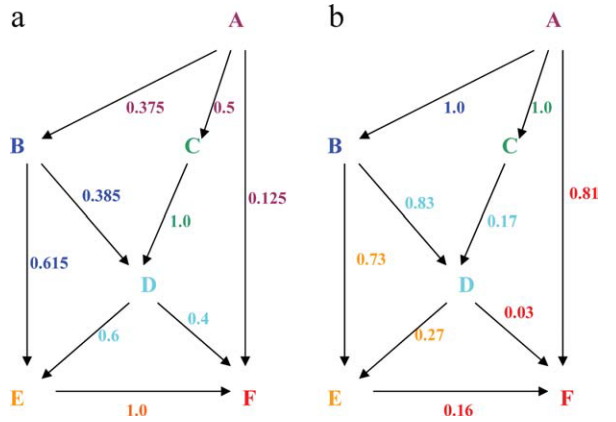

Figure 3. Flux normalization procedure to calculate pathway activity.

(a) outflux of species on pathways from species A are normalized, and (b) influx of species on pathways to species F are normalized. [Color figure can be viewed in the online issue, which is available at wileyonlinelibrary.com.]

After the weight of each connection is calculated, pathway weights are obtained by multiplying each connection weight in the pathway. When consumption pathways, i.e., pathways from certain species, are examined, normalized outflux values of species on the pathway are multiplied. When production pathways, i.e., pathways to specific species, are evaluated, normalized influx values of the species on the pathway are used in multiplication. Scaled pathway weights of the system in Figure 2 are shown in Table 3. The scaled pathway weights measure the contribution of each pathway to the consumption of this specific specie, while scaled weights of pathways to certain species weigh the contribution of each pathway to the production of this specific

Table 3. Scaled Pathway Weights of the System Shown in Figure 2

	Pathways	Weights of Pathways From A	Weights of Pathways to F
1	ABDF	5.78%	2.49%
2	ACDF	20.00%	0.51%
3	ABDEF	8.66%	3.59%
4	ACDEF	30.00%	0.73%
5	ABEF	23.06%	11.68%
6	AF	12.50%	81.00%
Total		100.0%	100.0%

Table 4. Characteristic Pathways of Methyl Butanoate and *n*-pentane Combustion

	Pathway	Scaled Pathway Weight	
		$T_0 = 650$ K	$T_0 = 950$ K
Methyl butanoate	MB → MB2J → MP2D → C2H3CO → C2H3 → C2H2 → HCCO → CO → CO2	46.19%	46.74%
	MB → MB2J → MB2OO → MB2OOH4J → MB2OOH4OO → MB4OOH2*O → MP3J2*O → CH3OCO → CH3O → HCO → CO → CO2	10.22%	3.01%
	MB → MB2J → MB2OO → MB2OOH4J → MBCY4O2 → MP2D → C2H3CO → C2H3 → C2H2 → HCCO → CO → CO2	7.31%	4.12%
	MB → MBMJ → NC3H7CO → NC3H7 → C2H4 → C2H3 → C2H2 → HCCO → CO → CO2	6.83%	8.88%
	MB → MBMJ → MBMOO → MBMOOH2J → MBCY2OM → SC3H5OCH2 → C3H5-S → C2H2 → HCCO → CO → CO2	5.38%	3.17%
N-pentane	NC5H12 → C5H11–2 → C5H11O2–2 → C5H10OOH2–4 → C5H10OOH2–4O2 → NC5KET24 → CH3COCH2 → CH2CO → HCCO → CO → CO2	15.96%	0.32%
	NC5H12 → C5H11–2 → C3H6 → C3H5-A → C3H4-A → C3H3 → C3H2 → HCCO → CO → CO2	37.88%	81.12%
	NC5H12 → C5H11–2 → C5H11O2–2 → C5H10OOH2–4 → C5H10O2–4 → CH3CO → CO → CO2	27.16%	1.01%

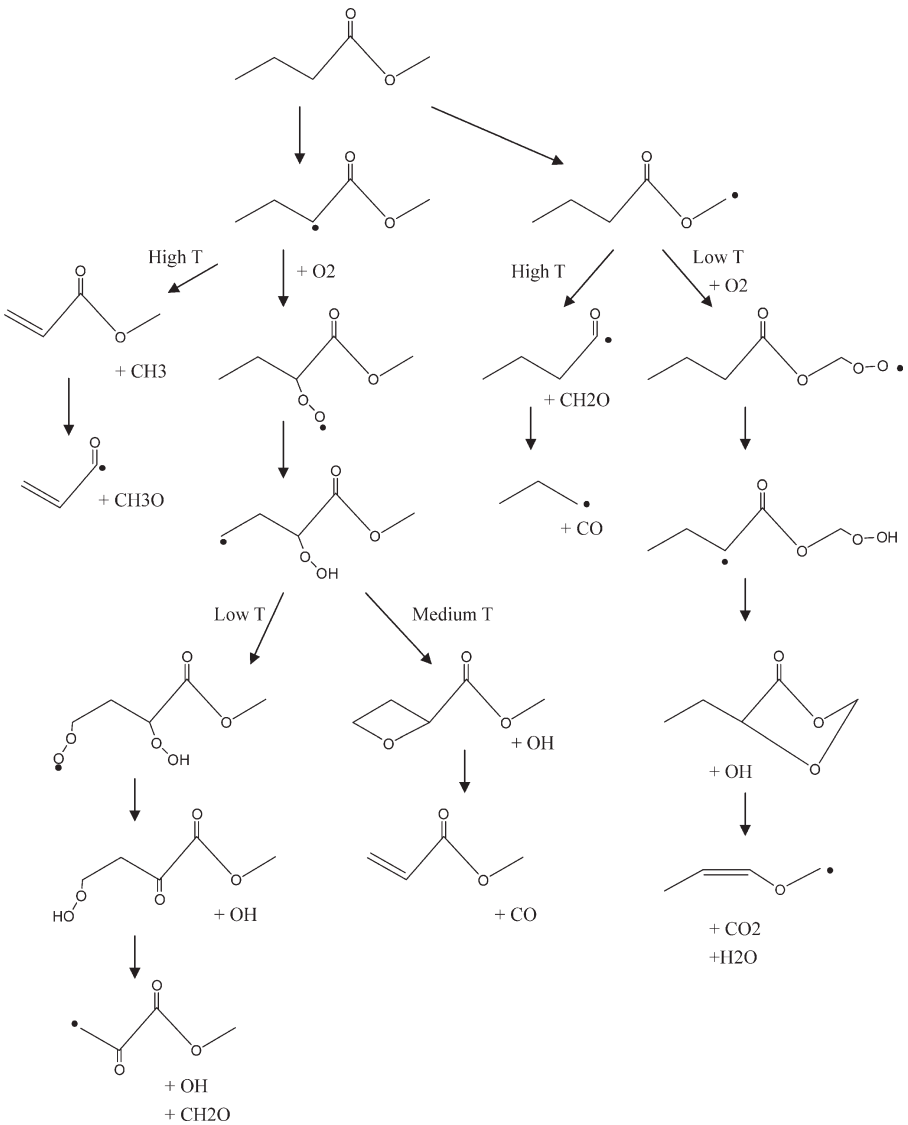

Figure 4. Characteristic pathways of methyl butanoate oxidation identified by carbon flux analysis.

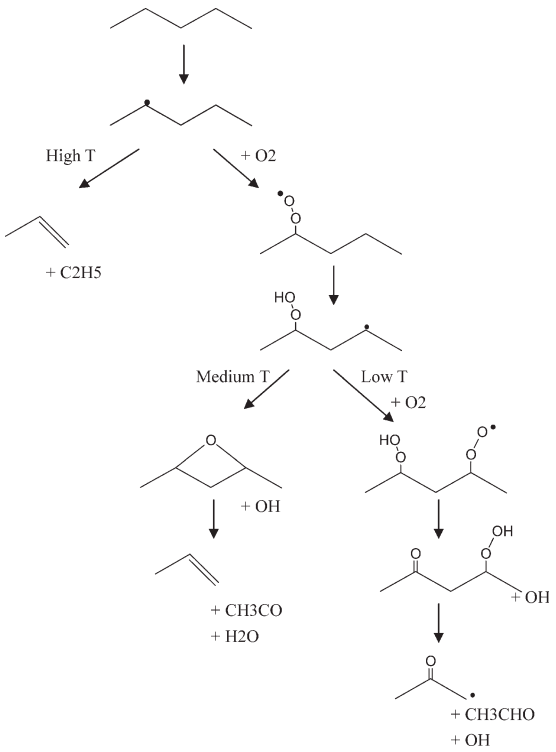

Figure 5. Characteristic pathways of *n*-pentane oxidation identified by carbon flux analysis.

specie. Thus for the example considered in Figure 2, the pathway activity in Table 3 can be interpreted in the following way. Pathway ACDEF makes the largest contribution to the consumption of species A and has a weight of 30%, while pathway AF is the most important pathway in the production of species F with an 80% contribution. The pathway weights are normalized to the value of 1, which enables direct comparison of pathway activity between different systems.

To demonstrate the pathway analysis method in complex kinetic mechanisms, the proposed method is applied on the methyl butanoate and *n*-pentane mechanisms. In the searching step, methyl butanoate and *n*-pentane are considered as initial species to analyze fuel oxidation pathways. A total of 356 pathways are identified for *n*-pentane oxidation and 293 pathways for methyl-butanoate. However, due to the limitations of space, only few characteristic pathways are shown in Table 4. The contribution of different pathways to the oxidation of original reactants can be interpreted from the pathway activities. The pathways summarized in Table 4 involve various regimes such as second oxygen addition, hydroperoxyalkyl radical decomposition, and beta scission. The competition between different regimes is shown in Figures 4 and 5. As shown in Figure 4, in addition to different oxidation pathways, competition also exists between the decomposition of carbon chain and methoxyl group, which makes the methyl butanoate oxidation more complicated than *n*-pentane oxidation. Based on the results shown in Table 4, it is found that the preferential oxidation pathway of methyl butanoate is through the hydrogen abstraction from the carbon chain (Pathways 1–3) rather than the methoxyl group (Pathways 4 and 5). At both temperatures (650 K and 950 K) the combined contribution of pathways from hydrogen abstraction on the carbon chain (63.72% at 650 K and 53.87% at 950 K) are much larger than that of pathways from hydrogen abstraction on the methoxyl group (12.21% at 650 K and 12.05% at 950 K). Lacking an ester group, *n*-pentane has less complicated oxidation pathways. At 650 K, three major pathways are identified, with beta scission the most important (37.88%), followed by second oxygen addition (15.96%) and hydroperoxyalkyl decomposition (27.16%). The competition favors beta scission as the temperature increases. The scaled pathway weights indicate that beta scission accounts for 81.12% of *n*-pentane oxidation at 950 K while second oxygen addition and hydroperoxyalkyl decomposition exhibit very small activities (0.32% and 1.01%).

The pathway analysis of the system reveals the element transformation network each described by a distinct and unique sets of characteristic pathways. Given all pathways, the reaction network can be visualized in the form of a flux graph with nodes representing mechanism species and edges denoting the element transformation between nodes. Figures 6a and 7a summarize carbon transformation network of methyl butanoate oxidation and *n*-pentane oxidation, respectively. The pathways depicted in the flux graphs correspond to the most significant species and element transformations as identified through time-integrated flux analysis. If the flux graph is coupled with instantaneous flux analysis, the network can be visualized in a dynamic mode with the edge weights a function of time which depend on which stage of the pathways is active. Figures 6b and 7b depict species with large flux at different stages of ignition process. Different sets of active species are identified and the evolution of the network can be captured. Therefore, by visualizing the evolution of the flux graphs, we understand the temporal evolution of chemistry. The novelty of our approach is that we do not simply define a static graph representation of a chemical mechanism but rather the dynamic evolution of the reaction pathways, thus enabling the monitoring of the activation/deactivation of critical pathways as a function of time.

Reactivity status indicator: a compact representation of chemical status

In previous sections, we have introduced two kinetic analysis approaches targeting species and pathways, respectively. Based on these two approaches, the chemical status of any reacting system can be fully captured by element fluxes of all source-sink pairs and the weights of all pathways. However, for a complex kinetic mechanism which involves thousands of species and tens of thousands of reactions, representation of chemistry by either of these two approaches is too expensive to compute, store, and interpret due to the fact that for every computational unit (time step and computational cell) in a flow calculation a high-dimensional vector (flux vector or pathway weight vector) is needed. To represent, analyze, and visualize effectively the chemical status of the system, we introduce a novel approach that arrives at a compact representation of the information content of these

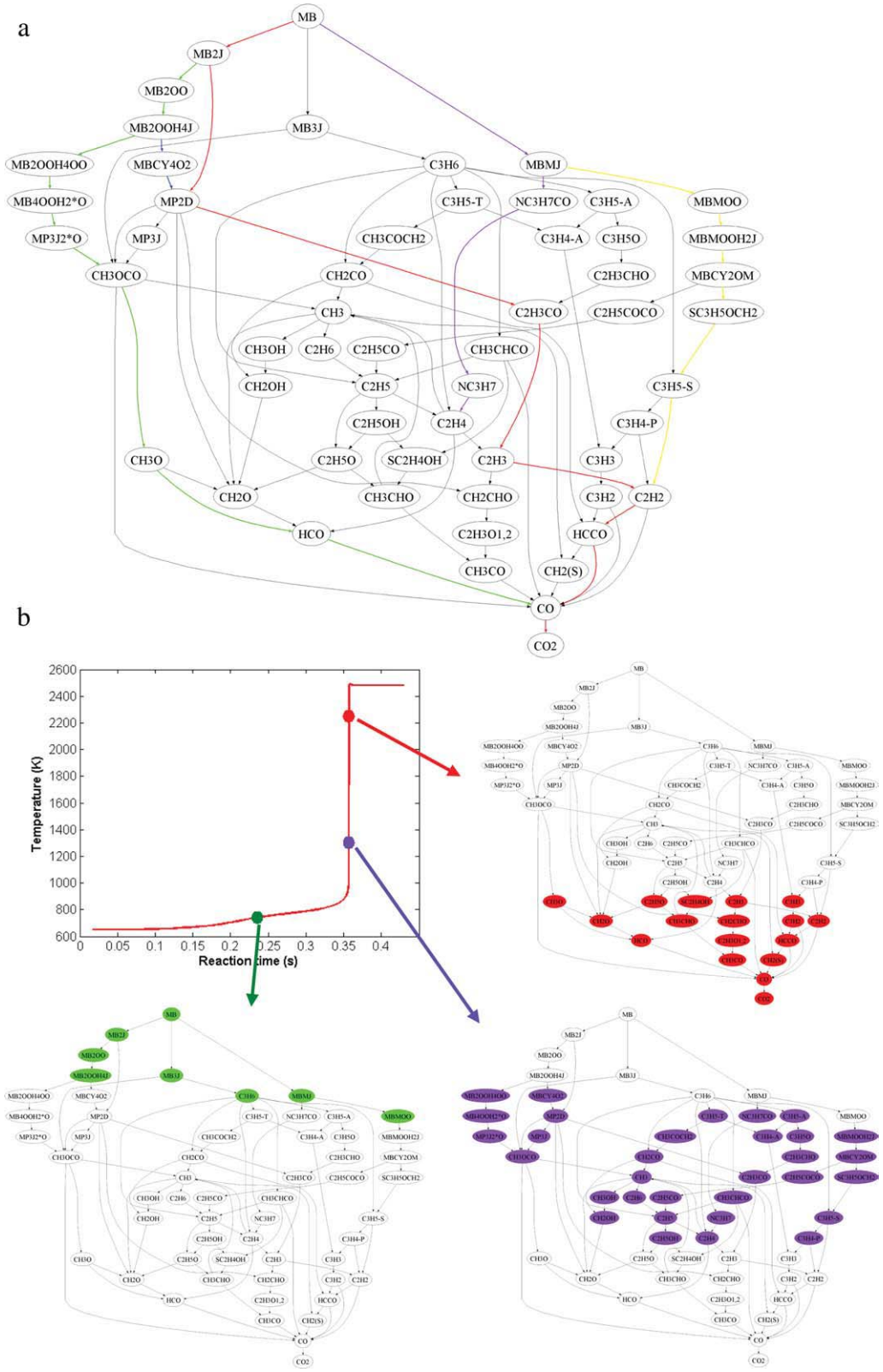

Figure 6. Carbon transformation network of methyl butanoate (MB) oxidation and its dynamic evolution in the reaction process.

(a) Characteristic pathways are highlighted with bold and color edges. (b) active species at different stages are highlighted, $T0 = 650$ K, $P0 = 9.6$ atm, $\phi = 1.0$. [Color figure can be viewed in the online issue, which is available at wileyonlinelibrary.com.]

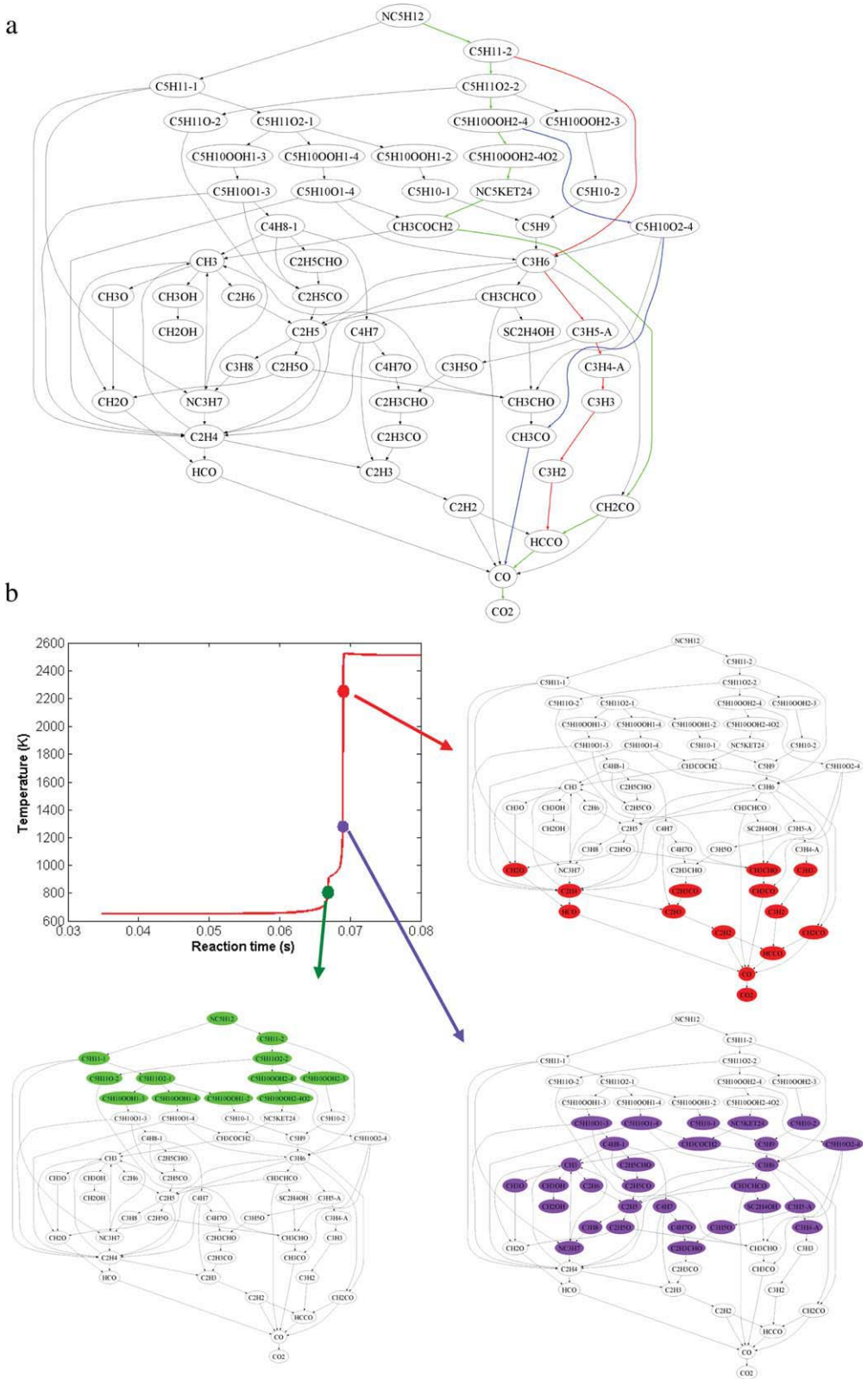

Figure 7. Carbon transformation network of *n*-pentane oxidation and its dynamic evolution in the reaction process.

(a) Characteristic pathways are highlighted with bold and color edges. (b) active species at different stages are highlighted, $T0 = 650$ K, $P0 = 9.6$ atm, $\phi = 1.0$. [Color figure can be viewed in the online issue, which is available at wileyonlinelibrary.com.]

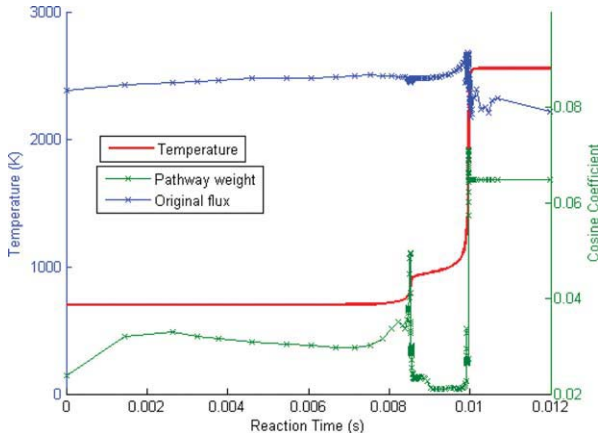

Figure 8. Cosine coefficient calculated based on pathway weights and original fluxes.

Data obtained for *n*-heptane oxidation in a PFR model. Initial temperature: 750 K; equivalence ratio: 1.0. [Color figure can be viewed in the online issue, which is available at wileyonlinelibrary.com.]

multi-dimensional vectors. This approach allows the projection of the totality of the information contained in temperature, pressure, species compositions, element fluxes, and pathway weights onto a single scalar. In doing so, multi-dimensional data can be first streamed from the temporally and spatially evolving chemical system, and these data are further processed and assigned a scalar "reactivity index." These reactivity indexes allow quick identification of the chemical status of the system at different time points and/or geometric regions.

To arrive at a compact representation of chemistry, we employ cosine coefficient,[22] to project a multi-dimensional vector onto a scalar. The metric based on cosine coefficient provides a normalized measure for similarity between two multi-dimensional vectors, thus it is widely used in data mining and clustering.[27,28] This cosine coefficient metric evaluates the similarity between any two vectors with same number of dimensions. Therefore, a unit vector is used as a basis to assign each multi-dimensional vector a cosine coefficient. During a reactive simulation, temperature, pressure, and species compositions, or element fluxes, or pathway weights are steamed from reactive flow simulations as "pseudo time series" evolving in time and space. Then for each of the streamed multi-dimensional vector, its cosine similarity between the basis vector is calculated and assigned to current system state. The outcome of this procedure is an integer representing the local chemical status of the system which we called "reactivity status indicator."

Figure 8 compares the cosine coefficient calculated based on fluxes and pathway weights for *n*-heptane combustion in a PFR model. It can be noticed that cosine coefficient of pathway weights is more representative of the state of the system than that of original fluxes. This is due to the fact that in original flux, a few species pairs such as CO to CO_2 have much higher flux than other species, which makes these few species dominant in the cosine coefficient calculation. While in pathway weights, since outflux and influx of each specie are normalized, the impact of large fluxes is eliminated. Therefore, cosine coefficient based on pathway

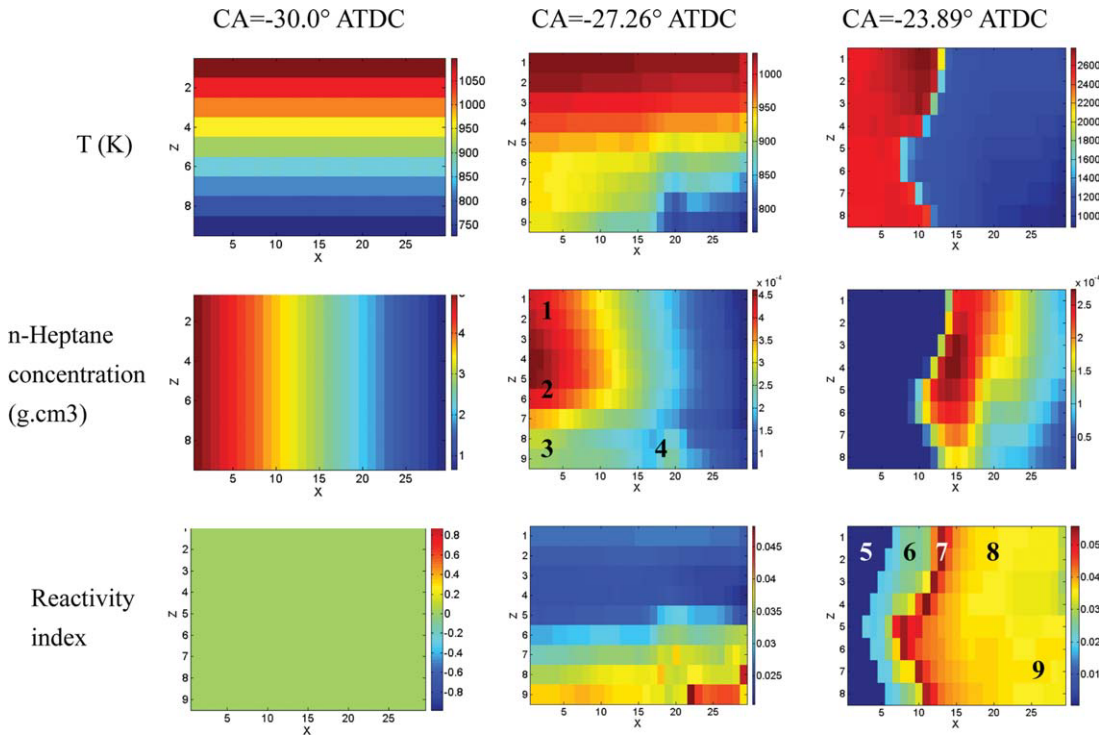

Figure 9. Temperature, *n*-heptane concentration, and reactivity index in HCCI engine chamber simulated in KIVA-3V.

[Color figure can be viewed in the online issue, which is available at wileyonlinelibrary.com.]

Table 5. Leading Pathways of Regions 2–4 in HCCI Engine Chamber at CA = −27.26° ATDC

	Pathway	Pathway Weight
Region 2	NC7H16 → C7H15–1 → C7H15O2–1 → C7H14OOH1–4 → C7H14O1–4 → CH2CHO → CH3CO → CO → CO2	5.71%
	NC7H16 → C7H15–2 → C5H11–1 → C2H4 → HCO → CO → CO2	4.89%
	NC7H16 → C7H15–2 → C7H15O2–2 → C7H14OOH2–5 → C7H14O2–5 → CH3COCH2 → CH2CO → HCCO → CO → CO2	4.16%
Region 3	NC7H16 → C7H15–2 → C7H15O2–2 → C7H14OOH2–4 → C7H14OOH2–4O2 → NC7KET24 → NC3H7CHO → NC3H7 → CH3 → CH2O → HCO → CO → CO2	2.08%
	NC7H16 → C7H15–1 → C7H15O2–1 → C7H14OOH1–4 → C7H14O1–4 → CH2CHO → CH3CO → CO → CO2	1.55%
	NC7H16 → C7H15–3 → C7H15O2–3 → C7H14OOH3–5 → C7H14OOH3–5O2 → NC7KET35 → C2H5 → C2H4 → HCO → CO → CO2	1.37%
Region 4	NC7H16 → C7H15–1 → C7H15O2–1 → C7H14OOH1–4 → C7H14O1–4 → CH2CHO → CH3CO → CO → CO2	1.87%
	NC7H16 → C7H15–2 → C7H15O2–2 → C7H14OOH2–4 → C7H14OOH2–4O2 → NC7KET24 → NC3H7CHO → NC3H7 → CH3 → CH2O → HCO → CO → CO2	1.48%
	NC7H16 → C7H15–3 → C7H15O2–3 → C7H14OOH3–5 → C7H14OOH3–5O2 → NC7KET35 → C2H5 → C2H4 → HCO → CO → CO2	1.32%

weights better distinguishes the difference between two system states, and thus better serves our purpose to derive a reactivity index to represent chemical status.

The calculation of the reaction state indicator is performed for an HCCI engine combustion simulated in KIVA-3V. The reaction state indicator is derived for each computational cell at each time step and is shown in Figure 9 for different time steps. An idealized case is used in this study, with initial temperature ranging from 750 K to 1100 K and initial equivalence ratio ranging from 0.2 to 1.6. During compression, cool flame behavior was observed at region 3 which corresponds to initial temperature 750 K. Fuel was consumed and temperature was increased to similar level of Region 2. This cool flame behavior is well captured by the reaction state indicators since at this region is much larger than the rest portion of the chamber. Another observation is that regions with the same initial temperature have similar reaction status than two regions with the same equivalence ratio. Considering regions 2, 3, and 4 for example, Region 2 and Region 3 have the same equivalence ratio but different initial temperatures while Region 3 and Region 4 have the same initial temperature but different equivalence ratios. As indicated by the reactivity status indicator, Region 3 and Region 4 are more similar than Region 2 and Region 3. This conclusion is also demonstrated by pathway analysis for these three regions. Leading pathways and their weights at these three regions are compared in Table 5. The results indicate that Region 3 and Region 4 have very similar leading pathways, while Region 2 is characterized by different set of active pathways. Leading pathways of Regions 2-4 are also depicted in the flux graph of *n*-heptane oxidation in Figures 10–12. As shown in Figures 11 and 12 active parts of the flux graphs of Region 3 and Region 4 largely overlap but Region 2 has a different set of active pathways, as shown in Figure 10.

When the chamber is ignited and the flame propagates, reactivity index divides the chamber into four regions. A thin region with the largest reactivity index is the flame front. In front of flame front is the un-ignited region which has elevated reactivity index and is ready to be ignited. Right behind the flame front is the postignition region where some remainder oxidation reactions are taking place. Behind the postignition region is the area where ignition is complete and all reactions are finished, resulting in lowest reactivity index. We also performed flux analysis for these four different regions (Regions 5-9 in Figure 9). Leading species transitions are listed in Table 6. In Region 7, the flame front, the production of CO_2 dominates the reaction system. Similar leading transitions were observed in Region 6 but with much smaller flux. While in Region 5, all reactions are nearly completed and very small fluxes were observed. In the un-ignited region (Regions 8 and 9), fuel oxidation and intermediate molecules production are the most active parts in the

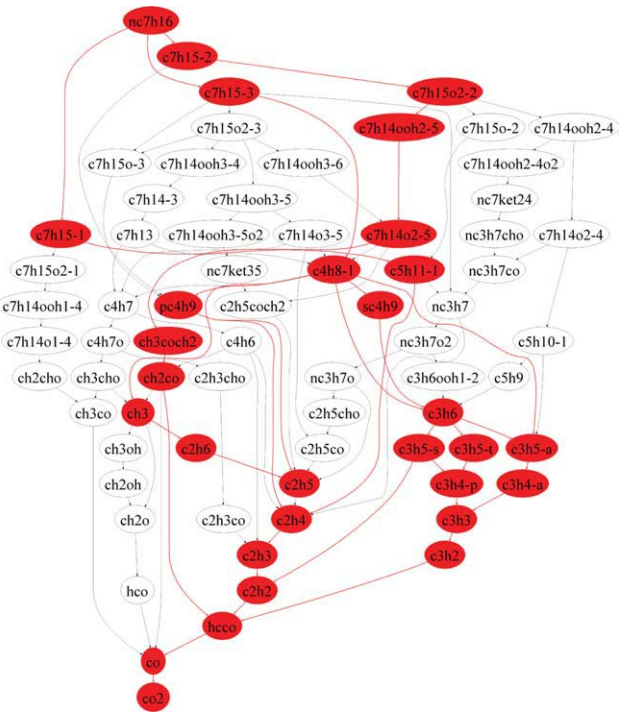

Figure 10. Active pathways of *n*-heptane oxidation in Region 2 of the engine chamber (as indicated in Figure 9).

[Color figure can be viewed in the online issue, which is available at wileyonlinelibrary.com.]

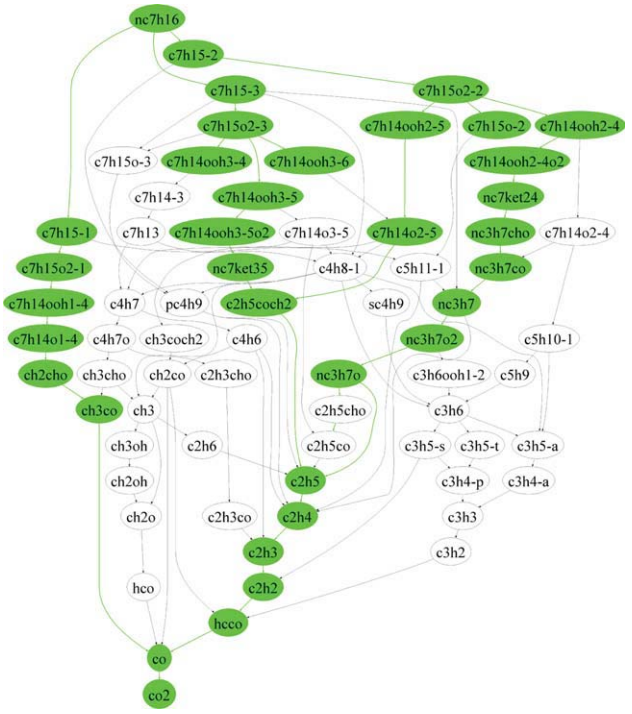

Figure 11. Active pathways of *n*-heptane oxidation in Region 3 of the engine chamber (as indicated in Figure 9).

[Color figure can be viewed in the online issue, which is available at wileyonlinelibrary.com.]

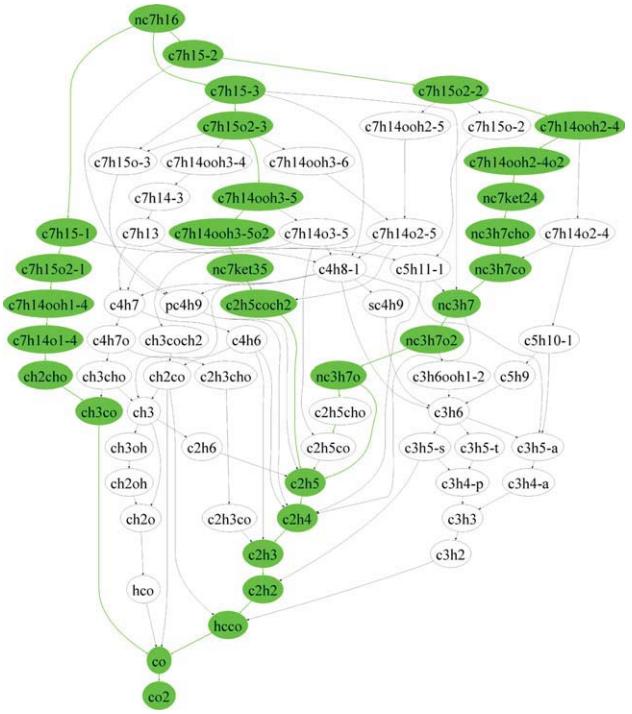

Figure 12. Active pathways of *n*-heptane oxidation in Region 4 of the engine chamber (as indicated in Figure 9).

[Color figure can be viewed in the online issue, which is available at wileyonlinelibrary.com.]

Table 6. Leading Carbon Fluxes of Region 5–9 in HCCI Engine Chamber at CA = −23.89° ATDC

	n-Heptane Oxidation		
	From	To	C Flux
Region 5	CO	CO2	5.38E-06
	HCCO	HCO	2.93E-06
	CH3CO	CO	2.37E-06
	C3H5-A	C3H4-A	1.74E-07
	C3H5-S	C3H4-P	9.35E-08
Region 6	CO	CO2	5.18E+01
	HCO	CO	4.32E+00
	HCCO	CO	3.73E+00
	CH3O	CH2O	8.91E-01
	CH2O	HCO	7.47E-01
Region 7	CO	CO2	3.26E+05
	HCO	CO	5.32E+03
	HCCO	CO	4.58E+03
	CH3O	CH2O	4.31E+03
	CH2O	HCO	3.95E+02
Region 8	C3H6	C3H5-A	6.33E+02
	CH3COCH2	CH2CO	5.92E+02
	CH2CHO	C2H3O1,2	5.57E+02
	CH3CHCO	C2H5	4.89E+02
	CH3CO	CO	4.35E+02
Region 9	C3H6	C3H5-A	5.52E+02
	CH3COCH2	CH2CO	5.01E+02
	CH2CHO	C2H3O1,2	4.76E+02
	CH2CO	HCCO	3.93E+02
	CH3CO	CO	3.53E+02

reaction network, indicating that the system is at preignition stage. Although Regions 8 and 9 have different fuel concentrations, similar leading transitions were observed only with slight difference in flux magnitudes. If one interprets chemical status from temperature, only ignited region, flame front, and un-ignited region can be identified. From the flux values of Regions 5 and 6 it can be seen that the ignited region can be further divided due to different chemical activities. While from fuel concentration map, the un-ignited region can be divided into sub-regions with different fuel concentrations. However, as shown by the fluxes of Regions 8 and 9, these sub-regions have similar chemical status despite different fuel concentrations.

Concluding Remarks

This article presented a computer program that performs fundamental kinetic analysis of complex reaction mechanisms based on time-integrated and instantaneous element flux. The flux pointers are used for the analysis of species activities, correlation between species activity and system dynamics, and pathways activities. Four novel aspects of this flux-based kinetic analysis are illustrated:

(1) The analysis of species activities based on element flux which provides accurate representation of reactive propensity.

(2) The analysis enables automatic identification of pathways connecting specific species in the system. The coupling of flux analysis and graph visualization software allows the visual inspection of the reaction pathways.

(3) By employing a normalized in-flux and out-flux of each species in the pathway, the program is able to quantify the activity of the entire pathway.

(4) A compact representation of the chemistry is achieved by projecting the totality of information contained in pathway weights onto a scalar computing the cosine similarity between pathway weight vector and a base vector.

The proposed kinetic analysis framework retrieves species concentrations, temperature, and pressure from the simulation to carry out element flux calculations and subsequent kinetic analysis procedures. The proposed analysis can be easily extended to the analysis of other models and chemical mechanisms. By optimizing the flux computing algorithm, the CPU required for the analysis is reduced to a minimal level, which makes it easy to interface this program to other simulation programs.

Acknowledgments

The authors acknowledge financial support from ExxonMobil R&E Co., NSF CBET Grant 0730582, and ONR Contract N00014-06-10835.

Literature Cited

1. Curran HJ, Gaffuri P, Pitz WJ, Westbrook CK, Callahan CV, Dryer FL. *Oxidation of automotive primary reference fuels at elevated pressures*. Twenty-seventh Symposium (International) on Combustion, Boulder, CO, 1998.
2. Dagaut P, El Bakali A, Ristori A. The combustion of kerosene: experimental results and kinetic modelling using 1-to 3-component surrogate model fuels. *Fuel*. 2006;85:944–956.
3. Fisher EM, Pitz WJ, Curran HJ, Westbrook CK. Detailed chemical kinetic mechanisms for combustion of oxygenated fuels. *Proc Combust Inst*. 2000;28:1579–1586.
4. Herbinet O, Pitz WJ, Westbrook CK. Detailed chemical kinetic oxidation mechanism for a biodiesel surrogate. *Combust Flame*. 2008;154:507–528.
5. Korobeinichev OP, Shvartsberg VM, Shmakov AG. The chemistry of combustion of organophosphorus compounds. *Uspekhi Khimii*. 2007;76:1094–1121.
6. Li SC, Varatharajan B, Williams FA. Chemistry of JP-10 ignition. *AIAA J*. 2001;39:2351–2356.
7. Marinov NM. A detailed chemical kinetic model for high temperature ethanol oxidation. *Int J Chem Kinet*. 1999;31:183–220.
8. Westbrook CK, Pitz WJ, Curran HJ. Chemical kinetic modeling study of the effects of oxygenated hydrocarbons on soot emissions from diesel engines. *J Phys Chem A*. 2006;110:6912–6922.
9. Dacol DK, Rabitz H. Sensitivity analysis of stochastic kinetic-models. *J Math Phys*. 1984;25:2716–2727.
10. Kramer MA, Rabitz H, Calo JM, Kee RJ. Sensitivity analysis in chemical-kinetics—recent developments and computational comparisons. *Int J Chem Kinet*. 1984;16:559–578.
11. Rabitz H, Kramer MA, Dacol DK. Sensitivity analysis in chemical kinetics. *Annu Rev Phys Chem*. 1983;34:419–461.
12. Turanyi T. Applications of sensitivity analysis to combustion chemistry. *Reliab Eng Syst Safety*. 1997;57:41–48.
13. Turanyi T. Rate sensitivity analysis of a model of the Briggs-Rauscher reaction. *React Kinet Catal Lett*. 1991;45:235–241.
14. Caracotsios M, Stewart WE. Sensitivity analysis of initial-value problems with mixed odes and algebraic equations. *Comput Chem Eng*. 1985;9:359–365.
15. Yetter RA, Dryer FL, Rabitz H. Some interpretive aspects of elementary sensitivity gradients in combustion kinetics modeling. *Combust Flame*. 1985;59:107–133.
16. NIST. *NIST Xsenkplot: an interactive, graphical post-processor for numerical simulations of chemical kinetics*. NIST, USA, 1996. Available at: http://www.nist.gov/cstl Accessed Dec. 10, 2009.
17. Bendtsen AB, Glarborg P, Dam-Johansen K. Visualization methods in analysis of detailed chemical kinetics modelling. *Comput Chem*. 2001;25:161–170.
18. Kee RJ, Rupley FM, Meeks E, Miller JA. *CHEMKIN-III: A FORTRAN Chemical Kinetics Package For The Analysis Of Gas-Phase Chemical And Plasma Kinetics*. CA (United States): Sandia National Labs: Livermore, 1996.
19. Androulakis IP, Grenda JM, Bozzelli JW. Time-integrated pointers for enabling the analysis of detailed reaction mechanisms. *AICHE J*. 2004;50:2956–2970.
20. Revel J, Boettner JC, Cathonnet M, Bachman JS. Derivation of a global chemical kinetic mechanism for methane ignition and combustion. *Journal De Chimie Physique Et De Physico-Chimie Biologique*. 1994;91:365–382.
21. He K, Androulakis IP, Ierapetritou MG. On-the-fly reduction of kinetic mechanisms using element flux analysis. *Chem Eng Sci*. 2009;65:1173–1184.
22. He K, Ierapetritou MG, Androulakis IP. A graph-based approach to developing adaptive representations of complex reaction mechanisms. *Combust Flame*. 2008;155:585–604.
23. Turanyi T, Tomlin AS, Pilling MJ. On the error of the quasi-steady-state approximation. *J Phys Chem*. 1993;97:163–172.
24. He K, Androulakis IP, Ierapetritou MG. A multi-element flux analysis for the incorporation of detailed kinetic mechanisms in reactive simulations. *Energy Fuels*. 2009;24:309–317.
25. Curran HJ, Gaffuri P, Pitz WJ, Westbrook CK. A comprehensive modeling study of n-heptane oxidation. *Combust Flame*. 1998;114:149–177.
26. Dixon C. Temporal resolution using a breadth-first search algorithm. *Ann Math Artif Intell*. 1998;22:87–115.
27. Schultz M, Liberman M. *Topic Detection and Tracking using idf-Weighted Cosine Coefficient*. Philadelphia, PA (United States): University of Pennsylvania, 1999.
28. Tan PN, Steinbach M, Kumar V. *Introduction to Data Mining*. Reading, MA: Addison-Wesley, 2005:500–532.

Appendix A: Pseudo Code of Element Flux Analysis

Species participating in each reaction (K and K1) are identified and if two species contain the element of interest (pseudo code line 4 and line 8), we use the stoichiometric coefficients ISTOIC and ISTOIC1 to determine whether the two species have a reactant/product relationship (pseudo code line 10). Then the summation of the absolute values of forward and reverse reaction rates and number of atoms of element NELE in species K and K1 and this specific reaction determine the flux value between these two species (pseudo code line 15 and 16). The flux pointer for the two species AJK(IFROM, ITO, t) of current time step is created and stored.

- ICWKR: CHEMKIN work array containing all necessary information for describing the reactions and the associated thermodynamics
- NII: number of reactions in the mechanism
- MXSP: maximum species allowed per reaction
- ICNK: memory location defined by CHEMKIN
- ISTOIC: stoichiometirc coefficient
- NCF: CHEMKIN function determining whether species "K" contains element "NELE"
- Qfwd: array containing forward reaction rate calculated internally via CHEMKIN
- Qrev: array containing reverse reaction rate calculated internally via CHEMKIN

```
1. DO I = 1, NII
2.  DO N = 1, MXSP-1
3.   K = ICKWRK(ICNK + (I-1)*MXSP + N - 1)
4.    IF (K .NE. 0 .AND. NCF(NELE,K) .GT. 0) THEN
5.     ISTOIC = ICKWRK(ICNU + (I-1)*MXSP + N - 1)
6.      DO N1 = N+1, MXSP
7.       K1 = ICKWRK(ICNK + (I-1)*MXSP + N1 - 1)
8.        IF(K1 .NE. 0 .AND. NCF(NELE,K1) .GT. 0) THEN
```

```
      ISTOIC1 = ICKWRK(ICNU + (I-1)*MXSP +
     N1 - 1)
      IF(K.NE.K1.AND.ISTOIC*ISTOIC1.LT.0)
     THEN
        IFROM = K
        ITO = K1
        NAJ = ABS(ISTOIC)*NCF(NELE, IFROM)
       NAK = ABS(ISTOIC1)*NCF(NELE,ITO)
      AJK(IFROM, ITO, t) = AJK(IFROM, ITO, t) +
    (ABS(Qfwd(I))+ABS(Qrev(I)))*NAJ*NAK/
     (NAI(I))
    ENDIF
   ENDIF
  ENDDO
 ENDIF
ENDDO
ENDDO
```

Appendix B. Naming Conventions of the Methyl Butanoate and *n*-pentane Oxidation Mechanisms

mb=methyl butanoate
mp=methyl propanoate
me=methyl ethanoate
mm=methyl methanoate (=methyl formate)
ba= butanoic acid
Carbons are numbered starting with 1 = carbonyl carbon.

m denotes the carbon in the methoxy group.

Groups attached to a given carbon atom are listed after the number or letter labeling that carbon atom.

j denotes a radical site.

*o denotes an oxygen atom attached via a double bond.

For example, mb3j4ooh is methyl butanoate with a hydroxyl group attached to the terminal cabon (number 4) and a hydrogen atom missing from the carbon next to the terminal one (number 3)

d denotes a double bond connecting carbon n and carbon n+1.

For example, mb2d has a double bond between carbon 2 and carbon 3.

An example of a cyclic species is: mbcy4o2, which resembles mb but has an O bonded between carbons 4 and 2.

Note that in many cases a more conventional notation is used.

For example, ch3oco is used instead of mm1j. This is mainly for consistency with other reaction mechanisms.

Naming conventions are provided by Lawrence Livermore National Laboratory, which is also made available online:

https://www-pls.llnl.gov/data/docs/science_and_technology/chemistry/combustion/prf_glossary_v2.pdf

https://www-pls.llnl.gov/data/docs/science_and_technology/chemistry/combustion/mb_notes.txt

Manuscript received July 13, 2010, and final revision received Feb. 25, 2011.